Capacity of Distributed PHY-Layer Sensor Networks

Mischa Dohler, *Member, IEEE*, Athanasios Gkelias, *Student Member, IEEE*, and A. Hamid Aghvami, *Fellow, IEEE*

***Abstract*—Sensor networks are comprised of nodes with minimal baseband and RF functionalities. In such networks, it is assumed that a source sensor communicates with a target sensor over a number of relaying sensors by utilizing distributed low-complexity space-time encoding techniques, hence the resulting communication scenario is a generalized form of orthogonalized multiple-input multiple-output (MIMO) channels. The contributions of this paper are the derivation of the Shannon capacity in terms of natural units per second per Hertz for such space-time encoded distributed communication scenarios. Closed-form capacity expressions are derived for ergodic flat-fading Rayleigh and Nakagami channels, as well as the communication-rate outage probabilities for aforementioned channels. It is shown that the distributed Alamouti scheme yields the best performance over ergodic channels. In the case of nonergodic channels, the 3/4-rate sporadic space-time block code (STBC) is shown to give optimum performance. Finally, Monte Carlo simulations are used to assess the performance of distributed multistage sensor networks. It is shown that notable power savings can be achieved, compared to the traditional single-link sensor networks.**

***Index Terms*—Distributed information systems, multiple-input multiple-output (MIMO) systems, sensor networks.**

I. Introduction

THE CONCEPT of sensor networks is fairly new; therefore, little theoretical literature is available on them. Furthermore, there is no common consensus on the functionalities and inherent characteristics of sensor networks to date. Hence, in this paper, we assume that sensor networks have characteristics as described below.

Characteristics: The function of sensors is to sense certain features of their surroundings and pass this information to a unit that is capable of processing such data. The duty cycle of sensors is rather low, as is their data rate. The majority of the sensors are stationary, allowing for stable routing paths from the source sensors to the target sensor or processing unit. A primary concern for a sensor is for it to consume as little power as possible, as it has been envisaged that microscopic sensors will run on traditional batteries for months, if not for years. It is therefore a task of a sensor-network designer to allow for data transmission with minimal power consumption. This requirement translates directly to a high-capacity physical layer, where a certain data rate is accomplished with as little power consumption as possible.

Manuscript received April 2, 2004; revised August 16, 2005 and August 19, 2005. The review of this paper was coordinated by Prof. C. Lin.

M. Dohler is with France Télécom R&D, Meylan Cedex 38243, France (e-mail: Mischa.Dohler@francetelecom.com).

A. Gkelias and A. H. Aghvami are with Centre for Telecommunications Research, King's College London, London WC2B 5RL, U.K. (e-mail: athanasios.gkelias@kcl.ac.uk; hamid.aghvami@kcl.ac.uk).

Digital Object Identifier 10.1109/TVT.2005.863470

Background: Sensor networks are significantly different from traditional ad hoc networks. Firstly, the number of sensor nodes in a sensor network can be several orders of magnitude higher than the number of nodes in an ad hoc network. Moreover, sensor nodes are usually densely deployed, prone to failures, and limited in power provision, computational complexity, and memory. While most ad hoc networks communicate on a point-to-point basis, sensor nodes mainly use a broadcast communication paradigm, and they may not have a global identification [1]. There is a wide range of applications in which such networks might be used, such as environmental monitoring and control, robotic control and guidance in automatic manufacturing environments, military surveillance, interactive toys, smart homes providing security, identification, and personalization, and health monitoring [2], [3]. Recently, there has been a lot of interest in the building and deployment of sensor networks. Worth mentioning are the Wireless Integrated Network Sensors (WINS) [4] and SmartDust [5] projects, which aim to integrate sensing, computing, and wireless-communication capabilities into a small form factor to enable low-cost production of tiny sensor nodes in large numbers [6]. Concerning the physical layer of sensor networks, in [7], a physical-layer-driven approach to designing protocols, algorithms, and applications, which minimizes the energy consumption of sensor-network systems, is proposed. The energies consumed by M-ary and binary modulation are compared for their respective circuit power consumptions. M-ary modulation increases energy efficiency by reducing the transmission time of the device, but usually also increases the circuit complexity and power consumption. It has been observed [8] that diversity is most likely to be achieved in the frequency domain, since the static nature of the network and the single antenna on each sensor makes space or time diversity difficult to obtain. However, performance gains are observed if distributed space or time coding is deployed, as is demonstrated in this paper. In [3], methods are defined for the cooperative detection of targets by a distributed wireless sensor network, and for a cooperative transmission scheme of the results to a remote user. Some simple capacity calculations for the Gaussian case are also obtained, and finally, a simple phase rotation scheme that allows a variable number of transmitters without a common phase reference to attain gains using simple noncoherent combining is described. Regarding the medium access control (MAC), traditional wireless MAC protocols do not usually fit the requirements of a sensor network due to their unique resource constraints and application requirements [1].

Hence, some of the most notable solutions for sensor networks are the self-organizing MAC for sensor networks (SMACS) scheme and the eavesdrop and register (EAR) algorithms (both in [3]), the hybrid time division multiple access

(TDMA)/frequency division multiple access (FDMA)-based scheme in [7], and the carrier sense multiple access (CSMA)-based medium access in [10].

Since the main operating constraint for sensors is their available energy, any proposed solution for sensor networks must take energy considerations and energy savings into account. Power-aware and cost-aware metrics are the two main categories of metrics that have been devised to minimize power. Power-aware metrics aim to minimize the total power needed to route a message between two different locations, while cost-aware metrics look at methods to extend the nodes' battery lifetime [11]. In [2], a new power-aware routing protocol that is suitable for low-energy and low-bit-rate networks is described. As employed in this protocol, the use of a simple probabilistic forwarding mechanism to send traffic on different routes helps to use the node resources more efficiently; indeed, simulation results show an increase in network lifetime of up to 40% using this method. In [12], a dynamic power management (DMP) scheme is proposed, where the sensor node is turned off if no events occur. Such an event-driven power-consumption scheme is critical to maximize battery life. In [11], a number of power-aware (from a local point of view) routing protocols are evaluated. In these schemes, the routing protocol tries to make decisions using only information that is available from its neighboring nodes.

Also relevant to the current work are [9], [13]–[25], [35], which achieve performance benefits due to cooperative transmission and reception. The performed analysis therein and the proposed protocols demonstrate a diversity order equivalent to the total number or cooperating antenna elements.

Assumptions: In contrast to previously performed research, this paper accomplishes considerable power savings in a sensor network by utilizing distributed MIMO capacity techniques without cooperation between the nodes, hence minimizing the signaling and traffic load in the network [34]. Potential approaches here are to deploy space-time block codes (STBCs) [26]–[28], space-time trellis codes (STTCs) [29], or layered multiplexing [e.g., Bell Labs layered space-time architecture (BLAST)] [30]. Due to the severe power constraints, the simplest encoding strategy has been chosen, i.e., STBCs. The deployment of STBCs orthogonalizes the MIMO channel, and thus reduces it to an equivalent single-input single-output (SISO) channel [31], [32]. That is a very desirable property, both from the complexity as well as analysis point of view.

For operational simplicity, it is assumed that each sensor is in possession of one antenna element only, and the transceiver is capable of operating either in the TDMA or the FDMA mode. In the TDMA mode, each sensor receives data over the entire frequency band W and a frame duration T_1. After a possible processing, the data is retransmitted over the entire frequency band W and in a frame duration T_2, during which time it is not capable of receiving any data. In the FDMA mode, communication may occur continuously, but data are received in a fractional bandwidth W_1 and retransmitted in a fractional bandwidth W_2. Note that both of these bandwidths must not overlap.

As will be explained more thoroughly in Section II, the limitation of having just one antenna element per sensor reduces the distributed communication scenario at most to a multiple-input single-output (MISO) communication scenario. Also, since the sensors are spatially separated, no correlation will be observed, additionally simplifying the analysis. Finally, to facilitate the analysis, synchronization is assumed to be perfect.

Contributions: The contributions of this paper can be summarized as follows.

1) A closed capacity expression for the orthogonalized ergodic MISO Rayleigh and Nakagami flat-fading channels is derived, where the channel coefficients can have an arbitrary attenuation.
2) A closed capacity outage-probability expression for the orthogonalized ergodic MISO Rayleigh and Nakagami flat-fading channels is derived, where the channel coefficients can have an arbitrary attenuation.
3) The capacity behavior of multistage distributed sensor networks is assessed and simulated. The performance is compared to the nondistributed case and appropriate conclusions are drawn.

Paper Structure: In Section II, the system model is described in detail. The principle of a distributed (sensor) network is explained, as is the encoding/decoding strategy at each sensor. In Section III, the closed-form capacity expressions for orthogonalized ergodic MISO channels obeying Rayleigh and Nakagami fading distributions are derived. In Section IV, the respective outage probabilities are derived in closed form. The end-to-end ergodic capacity and capacity outage probability is studied in Section V. Here, a source sensor delivers information to a target sensor via a plurality of relaying sensors. Finally, conclusions are drawn in Section VI.

II. System Model

A. Principle of Distributed Sensor Networks

Given is a source sensor (s-S) that intends to deliver information to a target sensor (t-S) or processing unit via a given number of distributed relaying sensors (r-Ss), as depicted in Fig. 1. The s-S sends its information to a group of spatially adjacent r-Ss, which form the first-tier r-Ss. Since no cooperation between the nodes is allowed, the end-to-end diversity order is limited to the weakest relaying stage, which is the first stage. The achieved diversity order of 1 requires that the first-tier sensor nodes are spatially close to the s-S to minimize the power spent to reach the first tier.

The signal stream from the s-S is reached by the first-tier r-Ss, which space-time encode the data stream, i.e., each r-S transmits only a spatial fraction of the space-time code word such that the total output from the first-tier r-Ss comprises an MISO transmission. Since the MISO channel achieves a higher capacity and lower outage probability [39], the distance between the first and second relaying tier can be considerably larger than from the s-S to the first relaying tier, or alternatively, the transmission power can be reduced.

The second tier r-Ss receives the data stream, decodes it, and reencodes and retransmits it to the third-tier r-Ss in the same manner as described above. This process is continued until the t-S or the processing unit is reached. Note that it is not the aim of this paper to deal with the optimum data routing path

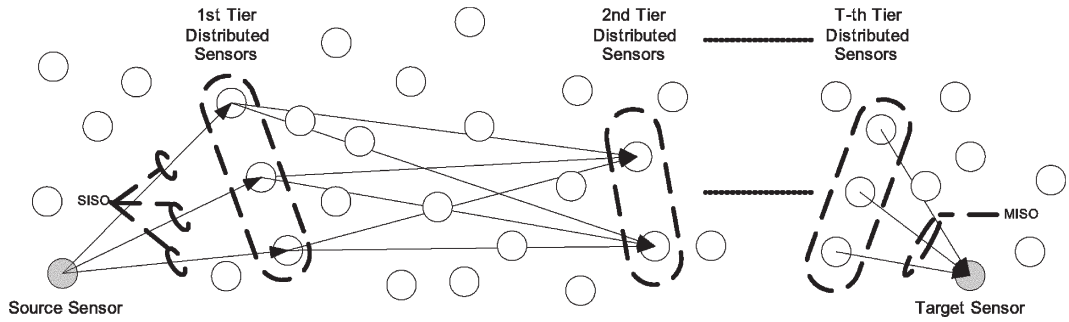

Fig. 1. Distributed sensor network, where a source sensor communicates with a target sensor via a number of sensor tiers, each of which is formed of distributed relaying sensors.

through the distributed sensor network; it is also assumed that the tiers of r-Ss are already formed and the sensors know about which spatial fraction of a space-time code word they have to (re-)transmit. The distributed encoding process is described in more detail as follows, where an FDMA-based relaying system with T relaying sensor tiers is assumed.

Source Sensor: The s-S Gray maps b_0 source information bits onto symbol x by utilizing an M_0-phase-shift keying (PSK) [or M_0-quadratic-amplitude modulation (QAM)] signal constellation, where $b_0 = \log_2 M_0$. The data stream is transmitted on frequency band W_0 with power S_0.

First-Tier Relaying Sensors: The first-tier r-Ss receive the data on frequency band W_0, detect it, space-time encode it, and transmit it simultaneously on frequency band W_1 with a total power S_1. Each r-S Gray maps $K_1 b_1$ bits onto symbols $x_1, x_2, \ldots, x_K$ by utilizing an M_1-PSK (or M_1-QAM) signal constellation, where $b_1 = \log_2 M_1$ and K_1 is the number of symbols per space-time encoding.

The $\{x_k\}_{k=1}^{K_1}$ are encoded with an orthogonal space-time coding matrix $\mathcal{G}_1$ of size $p_1 \times d_1$, where p_1 is the number of symbol durations required to transmit the space-time code word, and d_1 is the number of distributed r-Ss (and therefore equivalent to the number of transmit antennas). At each time instant t, the encoded symbol $c_{t,i}$ with $t = 1, \ldots, p_1$ and $i = 1, \ldots, d_1$ is transmitted simultaneously from the ith distributed r-S. Clearly, the rate of the first-tier STBC is $R_1 = K_1/p_1$.

Tth-Tier Relaying Sensors: The Tth-tier r-Ss receive data on frequency band W_{T-1}, space-time decode it, space-time reencode it, and retransmit it on frequency band W_T with a total power S_T. The encoding procedure is the same as described above, where the rate of the STBC is R_T.

Target Sensor: The t-S receives the data on frequency band W_T, space-time decodes it, and performs the final detection. If the s-S deploys a channel code, e.g., a simple trellis code, then the t-S performs the equivalent channel decoding to boost performance.

Each relaying sensor tier clearly may use a different signal constellation and STBC. It is only of importance that the consecutive tier has knowledge of the transmission parameters of the previous tier.

B. Equivalent SISO Model

To improve readability, superscripts related to the respective relaying tier are omitted here. Given one relaying stage with n_{T} distributed transmit sensors and n_{R} distributed receive sensors. Because sensors of the same tier do not communicate among each other, there are n_{R} MISO channels with n_{T} transmit antennas. Also, because of the spatial separation between sensors, the rather low data rates generated by sensor networks, and the low mobility prevailing in indoor environments, the channel coefficients are assumed to be independent, frequency flat, and quasi-static. Without loss of generality, only one MISO channel from the n_r available is considered here. The channel matrix thus reduces to a $1 \times n_{\mathrm{T}}$ channel vector $\mathbf{h}$, and it is defined as

$$\mathbf{h} \triangleq (h_1, \ldots, h_{n_{\mathrm{T}}}) \tag{1}$$

where h_i, $i = (1, \ldots, n_{\mathrm{T}})$, denotes the channel gain from the ith transmit sensor to the receive sensor. The use of orthogonal STBCs is known to decouple the MIMO (here, MISO) channel into parallel SISO channels [31]–[33]. This property is henceforth referred to as an orthogonalization of the MIMO (here, MISO) channel. This advantageous property may come at a loss in transmission rate R, which is defined as

$$R \triangleq \frac{K}{p} \tag{2}$$

where K is the number of symbols per space-time encoding and p is the number of symbol durations required to transmit the space-time code word [33]. For fixed channel realizations $\mathbf{h}$, the normalized capacity in natural units per second per Hertz over such orthogonalized MISO channel can be expressed as [33]

$$C = R \log\left(1 + \frac{1}{R}\frac{\|\mathbf{h}\|^2}{n_{\mathrm{T}}}\frac{S}{N}\right) \tag{3}$$

where S is the average transmitted power and N is the noise power at the receiver. $\|\mathbf{h}\|$ denotes the Frobenius norm of $\mathbf{h}$, the square of which is given as

$$\|\mathbf{h}\|^2 = \sum_{i=1}^{n_{\mathrm{T}}} |h_i|^2 = \mathrm{tr}(\mathbf{h}\mathbf{h}^{\mathbf{H}}) \tag{4}$$

where the superscript $\mathbf{H}$ denotes the Hermitian operation and $\mathrm{tr}()$ is the trace operator. If the channel realizations $\mathbf{h}$ are

random, then the ergodic channel capacity is obtained by averaging over all channel conditions $\|\mathbf{h}\|^2 \triangleq \lambda$, i.e.,

$$C = \mathrm{E}_\lambda \left\{ R \log \left(1 + \frac{1}{R} \frac{\lambda}{n_\mathrm{T}} \frac{S}{N} \right) \right\} \tag{5}$$

$$= \int_0^\infty R \log \left(1 + \frac{1}{R} \frac{\lambda}{n_\mathrm{T}} \frac{S}{N} \right) f_\lambda(\lambda) d\lambda \tag{6}$$

where $\mathrm{E}_\lambda\{\cdot\}$ denotes the expectation with respect to λ with a probability density function (pdf) of $f_\lambda(\lambda)$.

Finally, the average signal-to-noise ratio (SNR) per symbol at detection can be expressed as [33]

$$\overline{\gamma} = \frac{1}{R} \frac{\mathrm{E}\left\{\|\mathbf{h}\|^2\right\}}{n_\mathrm{T}} \frac{S}{N}. \tag{7}$$

Defining $\mathrm{E}\{h_i h_i^*\} \triangleq \alpha_i^2,\ i = (1, \ldots, n_\mathrm{T})$, where the superscript * denotes the complex conjugate, then (7) can be rewritten as

$$\overline{\gamma} = \frac{1}{R} \frac{\sum_{i=1}^{n_\mathrm{T}} \alpha_i^2}{n_\mathrm{T}} \frac{S}{N} \tag{8}$$

which will be useful for subsequent analysis.

III. Ergodic Capacity of Orthogonalized Distributed MISO Channels

A. Capacity Integral

A closed-form expression for the Shannon capacity over ergodic Rayleigh flat-fading MIMO channels is presented here. It is utilized later in the paper to compare the capacity of a generic MISO channel with the capacity of an orthogonalized MISO channel. This derivation of the closed-form expression requires knowledge of the solution of the capacity integral, which is frequently encountered in calculating MIMO or MISO capacities.

The capacity C in natural units per second per Hertz of a normalized ergodic Rayleigh flat-fading MIMO channel with n_T transmit and n_R receive antennas constrained by power S was elegantly derived by Telatar [39] as

$$C = \int_0^\infty \log \left(1 + \frac{\lambda}{n_\mathrm{T}} \frac{S}{N} \right) \cdot \sum_{k=0}^{m-1} \frac{k!}{(k+n-m)!} \left[L_k^{n-m}(\lambda) \right]^2 \lambda^{n-m} \mathrm{e}^{-\lambda} d\lambda \tag{9}$$

where N is the received noise power, $m = \min\{n_\mathrm{R}, n_\mathrm{T}\}$, $n = \max\{n_\mathrm{R}, n_\mathrm{T}\}$, and $L_k^{n-m}(\lambda)$ is the associated Laguerre polynomial of order k. This can be conveniently expressed as

$$C = \mathrm{E}_\lambda \left\{ m \log \left(1 + \frac{\lambda}{n_\mathrm{T}} \frac{S}{N} \right) \right\} \tag{10}$$

with

$$f_\lambda(\lambda) = \frac{1}{m} \sum_{k=0}^{m-1} \frac{k!}{(k+n-m)!} \left[L_k^{n-m}(\lambda) \right]^2 \lambda^{n-m} \mathrm{e}^{-\lambda} \tag{11}$$

where $f_\lambda(\lambda)$ is the pdf of an unordered eigenvalue λ [39]. A closed-form expression in terms of finite sums for the capacity given in (9) was derived in [37] and is given as

$$C = \sum_{k=0}^{m-1} \frac{k!}{(k+d)!} \times \left[\sum_{l=0}^{k} A_l^2(k,d) \hat{C}_{2l+d}(\tau) + \sum_{l_1=0}^{k} \sum_{l_2=0, l_2 \neq l_1}^{k} (-1)^{l_1+l_2} A_{l_1}(k,d) A_{l_2}(k,d) \hat{C}_{l_1+l_2+d}(\tau) \right] \tag{12}$$

where $d \triangleq n-m$, $A_l(k,d) \triangleq (k+d)!/[(k-l)!(d+l)!l!]$, and $\tau \triangleq (1/n_\mathrm{T})(S/N)$. $\hat{C}_\zeta(\tau)$ is defined as

$$\hat{C}_\zeta(\tau) \triangleq \int_0^\infty \log(1+\tau x) x^\zeta \mathrm{e}^{-x} dx. \tag{13}$$

Because of its frequent occurrence, this expression is henceforth referred to as the capacity integral. The solution to the capacity integral is given as [37]

$$\hat{C}_\zeta(\tau) = \sum_{\mu=0}^{\zeta} \frac{\zeta!}{(\zeta-\mu)!} \left[(-1)^{\zeta-\mu-1} \left(\frac{1}{\tau} \right)^{\zeta-\mu} \mathrm{e}^{\frac{1}{\tau}} \mathrm{Ei}\left(\frac{-1}{\tau} \right) + \sum_{k=1}^{\zeta-\mu} (k-1)! \left(\frac{-1}{\tau} \right)^{\zeta-\mu-k} \right] \tag{14}$$

where $\mathrm{Ei}(y) \equiv \int_{-\infty}^{y} (\mathrm{e}^t/t) dt$ is the exponential integral. Hence, the capacity of a generic MISO channel can be expressed in closed form as

$$C = \frac{1}{\Gamma(n_\mathrm{T})} \cdot \hat{C}_{n_\mathrm{T}-1} \left(\frac{1}{n_\mathrm{T}} \frac{S}{N} \right) \tag{15}$$

where $\Gamma(x)$ is the complete gamma function.

B. Orthogonalized MISO Ergodic Capacity—Rayleigh Fading

Equal Channel Gains: If all channel gains are equal, then $\mathrm{E}\{h_1 h_1^*\} = \cdots = \mathrm{E}\{h_{n_\mathrm{T}} h_{n_\mathrm{T}}^*\} \equiv \alpha^2$. Clearly, $\mathbf{h}\mathbf{h}^\mathbf{H}$ has rank 1; therefore, the capacity-determining eigenvalue λ of $\mathbf{h}\mathbf{h}^\mathbf{H}$ [39] is equal to $\mathbf{h}\mathbf{h}^\mathbf{H}$, i.e., $\lambda = \mathbf{h}\mathbf{h}^\mathbf{H} = \|\mathbf{h}\|^2$. Because $\|\mathbf{h}\|^2$ has a central chi-square distribution with $2n_\mathrm{T}$ degrees of freedom and mean $\mathrm{E}\{\lambda\} = n_\mathrm{T}\alpha^2$, the pdf of λ can be expressed as [38]

$$f_\lambda(\lambda) = \frac{1}{\Gamma(n_\mathrm{T})} \frac{\lambda^{n_\mathrm{T}-1}}{(\alpha^2)^{n_\mathrm{T}}} \mathrm{e}^{-\frac{\lambda}{\alpha^2}}. \tag{16}$$

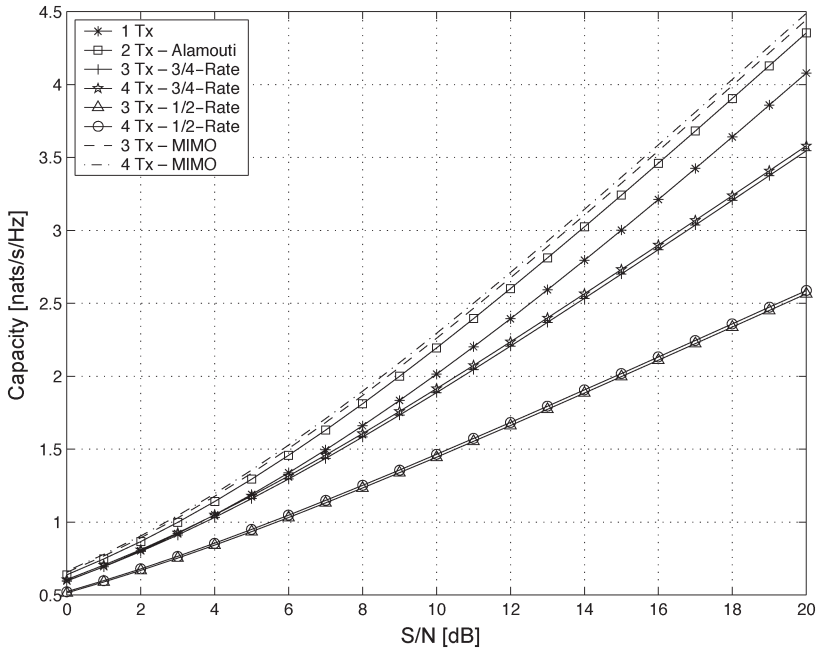

Fig. 2. Normalized Shannon capacity in natural units per second per Hertz versus S/N in decibels for various STBCs over an MISO Rayleigh channel with equal channel gains. $\alpha^2 = 1$.

With reference to (6) and some changes in variables, the capacity of the orthogonalized MISO channel can be expressed in closed form as

$$C = \frac{R}{\Gamma(n_{\mathrm{T}})} \int_0^{\infty} \log\left(1 + \lambda \frac{1}{R}\frac{\alpha^2}{n_{\mathrm{T}}}\frac{S}{N}\right) \lambda^{n_{\mathrm{T}}-1} \mathrm{e}^{-\lambda} d\lambda \quad (17)$$

$$= \frac{R}{\Gamma(n_{\mathrm{T}})} \cdot \hat{C}_{n_{\mathrm{T}}-1}\left(\frac{1}{R}\frac{\alpha^2}{n_{\mathrm{T}}}\frac{S}{N}\right)$$

$$= \frac{R}{\Gamma(n_{\mathrm{T}})} \cdot \hat{C}_{n_{\mathrm{T}}-1}\left(\frac{\overline{\gamma}}{n_{\mathrm{T}}}\right) \quad (18)$$

where $\overline{\gamma} = (\alpha^2/R)(S/N)$.

Fig. 2 depicts the normalized Shannon capacity in natural units per second per Hertz versus S/N in decibels for various MISO system configurations and $\alpha^2 = 1$. Depicted are the following cases: 1) $n_{\mathrm{T}} = 1$ (SISO); 2) $n_{\mathrm{T}} = 2$ (Alamouti); 3) $n_{\mathrm{T}} = 3$ (3/4 rate); 4) $n_{\mathrm{T}} = 4$ (3/4 rate); 5) $n_{\mathrm{T}} = 3$ (half-rate); 6) $n_{\mathrm{T}} = 4$ (half-rate); 7) $n_{\mathrm{T}} = 3$ (generic MISO); and 8) $n_{\mathrm{T}} = 4$ (generic MISO).

It can be observed that capacity increases for the generic MISO channels with an increasing number of transmit antennas. The same holds for the full-rate Alamouti STBC, which yields an asymptotic capacity gain of 0.3 nats/s/Hz, or equivalent power savings of 1.25 dB.

Interestingly, however, if the MISO channel is orthogonalized with the aid of half-rate or even 3/4-rate orthogonal STBCs, no capacity benefits can be observed. Note that the STBCs only orthogonalize the MISO channel; however, they do not give any coding gain. Therefore, if these bounds were to be approached, an outer channel code would have to be deployed.

Unequal Channel Gains: The capacity expression in closed form for the unequal channel gains is derived utilizing the moment generating function (MGF), which is defined as $\phi_\lambda(s) \triangleq \int_0^{\infty} \mathrm{e}^{s\lambda} f_\lambda(\lambda) d\lambda$ [40]. The MGF $\phi_{\lambda_i}(s)$ of the ith MISO Rayleigh channel with instantaneous power $\lambda_i \triangleq h_i h_i^*$ (and average power $\alpha_i^2 \triangleq \mathrm{E}\{h_i h_i^*\}$) can hence be derived as

$$\phi_{\lambda_i}(s) = \frac{1}{1 - s\alpha_i^2}. \quad (19)$$

The addition of the random channel gains according to (4) results in the convolution of their pdfs, which equates to the product of their MGFs. Therefore, the MGF of the MISO channel can be expressed as

$$\phi_\lambda(s) = \prod_{i=1}^{n_{\mathrm{T}}} \phi_{\lambda_i}(s) = \frac{1}{1 - s\alpha_1^2} \cdot \frac{1}{1 - s\alpha_2^2} \cdots \frac{1}{1 - s\alpha_{n_{\mathrm{T}}}^2}. \quad (20)$$

Resolving (20) into its partial fractions, one can write

$$\phi_\lambda(s) = \sum_{i=1}^{n_{\mathrm{T}}} K_i \phi_{\lambda_i}(s) \quad (21)$$

where the constants—poles of the MGF—are obtained by solving the set of linear equations, the solution to which is [44]

$$K_i = \prod_{i'=1, i' \neq i}^{n_{\mathrm{T}}} \frac{\alpha_i^2}{\alpha_i^2 - \alpha_{i'}^2}. \quad (22)$$

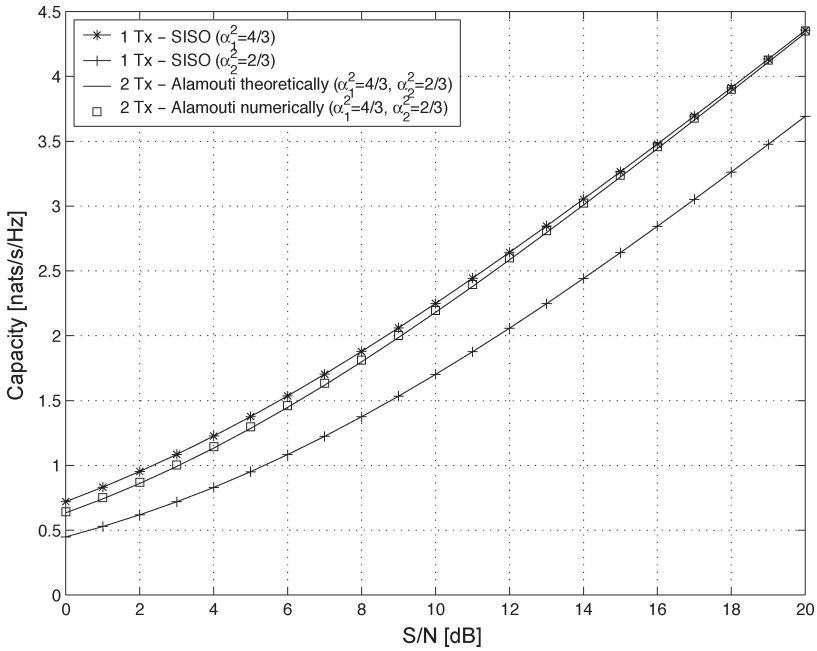

Fig. 3. Normalized Shannon capacity in natural units per second per Hertz versus S/N in decibels for the distributed Alamouti STBC over an MISO Rayleigh channel with unequal channel gains. $\alpha_1^2 = 4/3$ and $\alpha_2^2 = 2/3$.

The linearity of the inverse of the MGF therefore allows writing for the pdf of the eigenvalue $\lambda = \|\mathbf{h}\|^2$

$$f_\lambda(\lambda) = \sum_{i=1}^{n_\mathrm{T}} K_i \cdot \frac{1}{\alpha_i^2} \mathrm{e}^{-\frac{\lambda}{\alpha_i^2}}. \tag{23}$$

The capacity of the MISO link with unequal channel coefficients can finally be expressed in closed form as

$$C = R \sum_{i=1}^{n_\mathrm{T}} K_i \cdot \hat{C}_0 \left(\frac{1}{R} \frac{\alpha_i^2}{n_\mathrm{T}} \frac{S}{N} \right) = R \sum_{i=1}^{n_\mathrm{T}} K_i \cdot \hat{C}_0 \left(\overline{\gamma}_i \right). \tag{24}$$

Fig. 3 depicts the normalized Shannon capacity in natural units per second per Hertz versus S/N in decibels for the distributed Alamouti scheme. In the case of equal channel coefficients, the expectation of the square of the Frobenius norm of the normalized channel coefficients would yield n_T; here, $n_\mathrm{T} = 2$. For this reason, the power of the unequal channel coefficients is chosen such that $\alpha_1^2 + \alpha_2^2 \equiv 2$. Chosen was the particular case where $\alpha_1^2 : \alpha_2^2 = 2 : 1$, i.e., $\alpha_1^2 = 4/3$ and $\alpha_2^2 = 2/3$. Depicted are the cases where only channel with power α_1^2 is utilized, where only channel with power α_2^2 is utilized, and where the distributed Alamouti STBC is utilized. The latter is corroborated by numerical simulations.

Clearly, the loss in capacity of the distributed communication scenario is negligible compared to the case where communication happens through the stronger single link. However, a considerable capacity loss can be observed when the weaker single link is utilized. Therefore, when only a single link is deployed, then shadowing may severely degrade the link capacity, whereas when a distributed encoding is chosen, then the capacity is fairly robust to attenuations in either link. A quantification of the performance gains when independent shadowing dominates the communication system is postponed to Section V.

Fig. 4 depicts the normalized Shannon capacity in natural units per second per Hertz versus S/N in decibels for the distributed 3/4-rate STBC scheme. Here, the ratio between the channel coefficients was chosen such that $\alpha_1^2 : \alpha_2^2 : \alpha_3^2 = 4 : 2 : 1$, i.e., $\alpha_1^2 = 12/7$, $\alpha_2^2 = 6/7$, and $\alpha_3^2 = 3/7$. Again, severe capacity losses can be observed when communication happens only over the weaker single links; however, the distributed communication scenario offers a robust capacity. Note, however, that the absolute ergodic capacity of the 3/4-rate STBC is inferior to the ergodic capacity of the full-rate Alamouti scheme.

Fig. 5 depicts the normalized Shannon capacity in natural units per second per Hertz versus the normalized power in the first link α_1^2 for the distributed Alamouti scheme with $S/N = 10$ dB. Furthermore, depicted are the cases where communication happens only over either of the single links, where $\alpha_2^2 = 2 - \alpha_1^2$. The distributed Alamouti scheme outperforms even the strongest link for $0.8 < \alpha_1^2 < 1.2$. Notably, the capacity of the distributed scheme is much less dependent on the power of the individual links than in the case of the single-link schemes. Similar observations can be made for higher order STBCs. This corroborates the advantage of a distributed sensor network where channel conditions are not known *a priori* and feedback is limited.

Generic Channel Gains: Generally, the channel gains can be different where some gains are repeated. In this case, the MGF of the eigenvalue λ of the MISO channel can be expressed as

$$\begin{aligned} \phi_\lambda(s) &= \prod_{i=1}^{n_\mathrm{T}} \phi_{\lambda_i}(s) \\ &= \frac{1}{\left(1 - s\alpha_1^2\right)^{\nu_1}} \cdot \frac{1}{\left(1 - s\alpha_2^2\right)^{\nu_2}} \cdots \frac{1}{\left(1 - s\alpha_g^2\right)^{\nu_g}} \end{aligned} \tag{25}$$

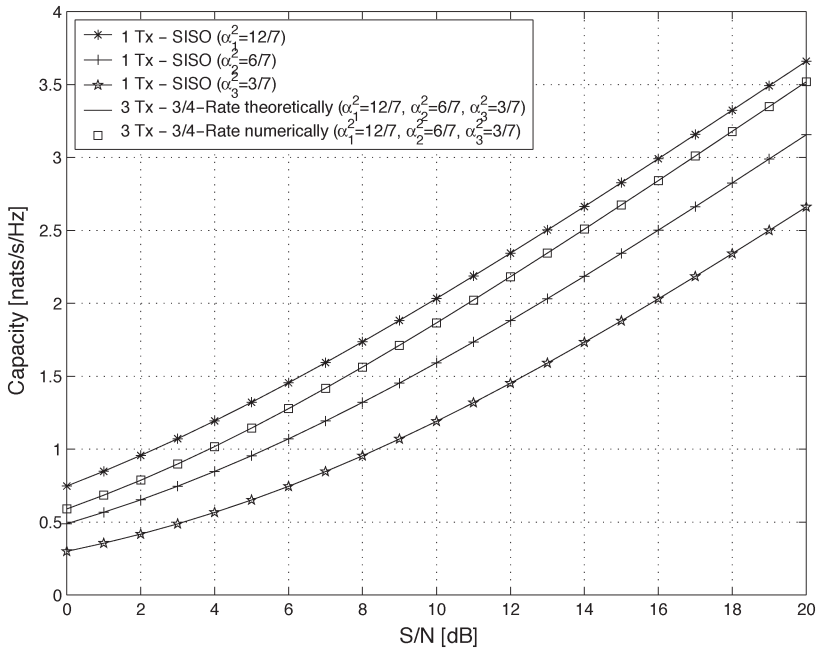

Fig. 4. Normalized Shannon capacity in natural units per second per Hertz versus S/N in decibels for the distributed 3/4-rate sporadic STBC over an MISO Rayleigh channel with unequal channel gains. $\alpha_1^2 = 12/7$, $\alpha_2^2 = 6/7$, and $\alpha_3^2 = 3/7$.

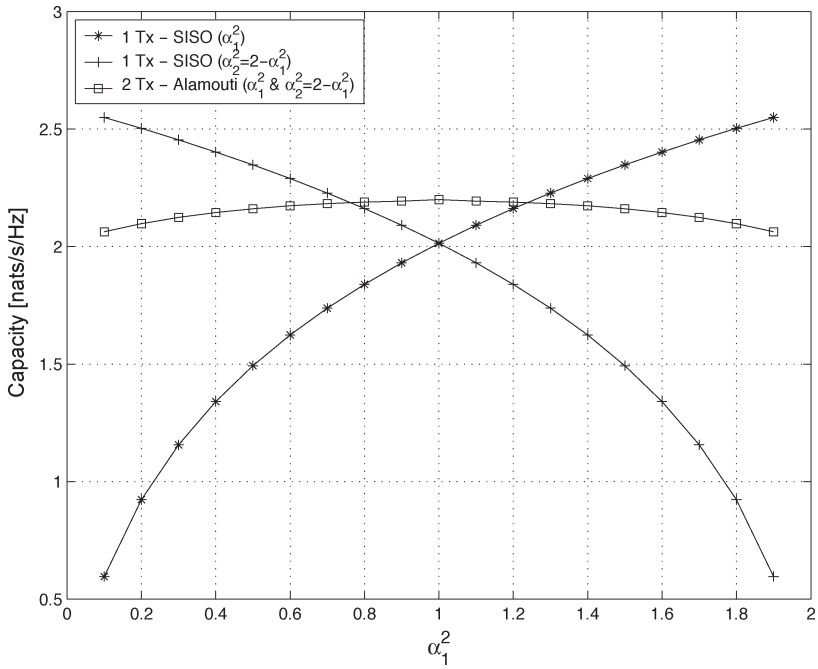

Fig. 5. Normalized Shannon capacity in natural units per second per Hertz versus the normalized power in the first link α_1^2 for the distributed Alamouti scheme over an MISO Rayleigh channel. $S/N = 10$ dB.

where g is the number of different channel coefficients, $\sum_{i=1}^{g} \nu_i \equiv n_{\mathrm{T}}$, and α_i^2, $i = (1, \ldots, g)$, is the distinct but possibly repeated average channel gains. Resolving (25) into its partial fractions with repeated roots yields

$$\phi_\lambda(s) = \sum_{i=1}^{g} \sum_{j=1}^{\nu_g} K_{i,j} \phi_{\lambda_i}^{j}(s). \tag{26}$$

In the Appendix, the coefficients $K_{i,j}$ are derived as

$$K_{i,j} = \frac{1}{(\nu_i - j)!\,(-\alpha_i^2)^{\nu_i - j}} \cdot \frac{\partial^{\nu_i - j}}{\partial s^{\nu_i - j}} \left[\prod_{i'=1, i' \neq i}^{g} \frac{1}{(1 - s\alpha_{i'}^2)^{\nu_{i'}}} \right]_{\frac{s=1}{\alpha_i^2}}. \tag{27}$$

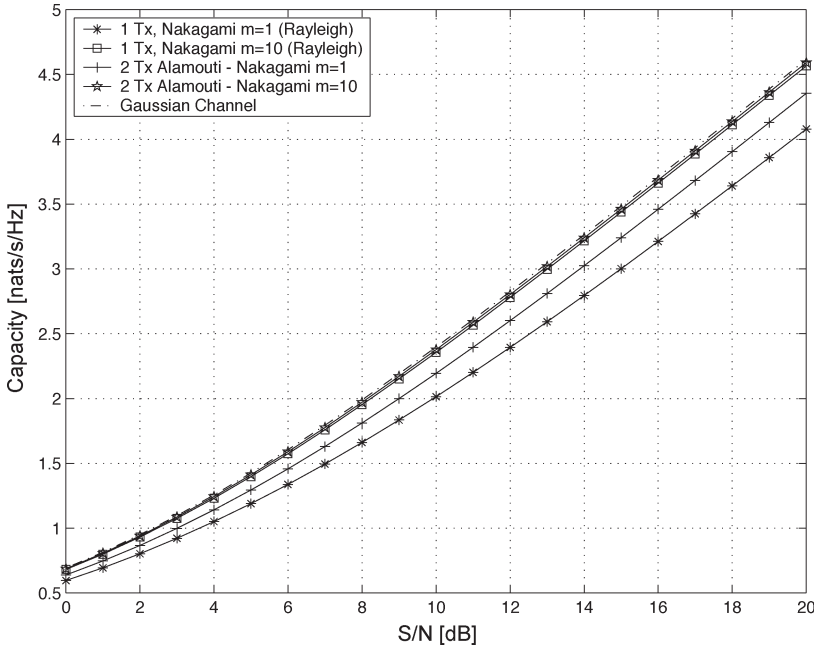

Fig. 6. Normalized Shannon capacity in natural units per second per Hertz versus S/N in decibels for the single-link case and the Alamouti scheme over an identically distributed MISO Nakagami channel with varying m factor; $\alpha^2 = 1$.

This allows one to express $f_\lambda(\lambda)$ in closed form as

$$f_\lambda(\lambda) = \sum_{i=1}^{g} \sum_{j=1}^{\nu_g} K_{i,j} \cdot \frac{\lambda^{j-1}}{\Gamma(j) \cdot (\alpha_i^2)^j} \mathrm{e}^{-\frac{\lambda}{\alpha_i^2}}. \tag{28}$$

The capacity of the generic MISO link can now be expressed in closed form as

$$C = R \sum_{i=1}^{g} \sum_{j=1}^{\nu_g} K_{i,j} \cdot \hat{C}_{j-1} \left(\frac{1}{R} \frac{\alpha_i^2}{n_\mathrm{T}} \frac{S}{N} \right) \tag{29}$$

$$= R \sum_{i=1}^{g} \sum_{j=1}^{\nu_g} K_{i,j} \cdot \hat{C}_{j-1}(\overline{\gamma}_i). \tag{30}$$

C. Orthogonalized MISO Ergodic Capacity—Nakagami Fading

Equal Channel Gains: The indoor fading distribution was often found to obey a Nakagami distribution [40], which is thus particularly important for indoor sensor networks. The pdf of the instantaneous power λ_i (and average power α_i^2) of the ith Nakagami channel can be expressed as [40]

$$f_{\lambda_i}(\lambda_i) = \frac{m_i^{m_i} \lambda_i^{m_i - 1}}{(\alpha_i^2)^{m_i} \Gamma(m_i)} \mathrm{e}^{-\frac{m_i \lambda_i}{\alpha_i^2}} \tag{31}$$

where m_i is the Nakagami m fading parameter of the ith channel ranging from $m_i = (1/2, \infty)$. Note that for $m_i = 1$, the Nakagami distribution turns into a Rayleigh distribution. Furthermore, the Ricean distribution with parameter K can be closely approximated with the Nakagami m distribution, where $m = (1+K)^2/(1+2K)$ [40].

The MGF of the instantaneous power of the ith Nakagami channel can be expressed as [40]

$$\phi_{\lambda_i}(s) = \frac{1}{\left(1 - s\frac{\alpha_i^2}{m_i}\right)^{m_i}}. \tag{32}$$

For n_T identically distributed Nakagami fading channels, i.e., $\alpha_1^2 = \cdots = \alpha_{n_\mathrm{T}}^2 = \alpha^2$ and $m_1 = \cdots = m_{n_\mathrm{T}} = m$, the MGF of the eigenvalue $\lambda = \|\mathbf{h}\|^2$ is therefore given as

$$\phi_\lambda(s) = \left[\frac{1}{\left(1 - s\frac{\alpha^2}{m}\right)^m} \right]^{n_\mathrm{T}} \tag{33}$$

the inverse of which leads to the desired pdf of the eigenvalue of a Nakagami-distributed MISO channel

$$f_\lambda(\lambda) = \frac{m^{mn_\mathrm{T}} \lambda^{mn_\mathrm{T}-1}}{(\alpha^2)^{mn_\mathrm{T}} \Gamma(mn_\mathrm{T})} \mathrm{e}^{-\frac{m\lambda}{\alpha^2}}. \tag{34}$$

The capacity for $m \in \mathbb{N}$ is solvable in closed form as

$$C = \frac{R}{\Gamma(mn_\mathrm{T})} \cdot \hat{C}_{mn_\mathrm{T}-1} \left(\frac{1}{R} \frac{\alpha^2}{mn_\mathrm{T}} \frac{S}{N} \right) \tag{35}$$

$$= \frac{R}{\Gamma(mn_\mathrm{T})} \cdot \hat{C}_{mn_\mathrm{T}-1} \left(\frac{\overline{\gamma}}{mn_\mathrm{T}} \right) \tag{36}$$

where $\overline{\gamma} = (\alpha^2/R)(S/N)$. Note that if $m \in \mathbb{R}$, then m should be replaced by $\lfloor m \rfloor$ to obtain a lower bound, i.e., the capacity that is at least achieved by the ergodic Nakagami MISO channel.

Fig. 6 depicts the normalized Shannon capacity in natural units per second per Hertz versus S/N in decibels for

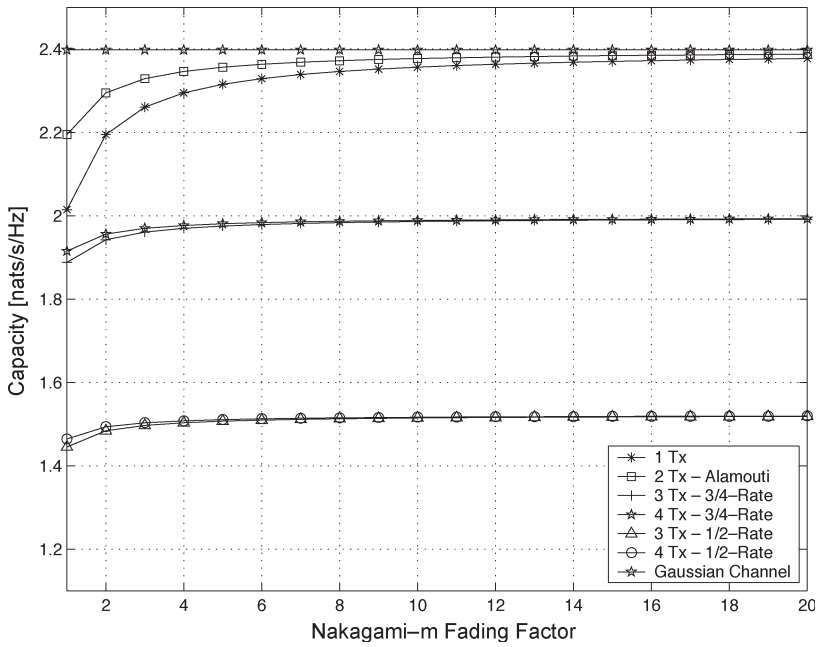

Fig. 7. Normalized Shannon capacity in natural units per second per Hertz versus the Nakagami m fading factor for various MISO system configurations. $S/N = 10$ dB and $\alpha^2 = 1$.

various MISO system configurations, and $\alpha^2 = 1$ over a Nakagami channel. Depicted are the following cases: 1) $n_{\mathrm{T}} = 1$ (SISO) with $m = 1$ (Rayleigh); 2) $n_{\mathrm{T}} = 1$ (SISO) with $m = 10$ (strong LOS); 3) $n_{\mathrm{T}} = 2$ (Alamouti) with $m = 1$ (Rayleigh); 4) $n_{\mathrm{T}} = 2$ (Alamouti) with $m = 10$ (strong LOS); and 5) Gaussian channel for comparison. Clearly, for $m = 10$, i.e., a strong LOS communication scenario, the capacity reaches Gaussian performance. This is independent from the number of transmit antennas as the fading channel exhibits very few fluctuations for high m.

Fig. 7 depicts the normalized Shannon capacity in natural units per second per Hertz versus the Nakagami m fading factor for various MISO system configurations: $S/N = 10$ dB and $\alpha^2 = 1$. The Nakagami m fading factor is varied from $m = 1$ (Rayleigh) to $m = 20$ (very strong LOS). Compared are the following scenarios: 1) $n_{\mathrm{T}} = 1$ (SISO); 2) $n_{\mathrm{T}} = 2$ (Alamouti); 3) $n_{\mathrm{T}} = 3$ (3/4 rate); 4) $n_{\mathrm{T}} = 4$ (3/4 rate); 5) $n_{\mathrm{T}} = 3$ (half-rate); 6) $n_{\mathrm{T}} = 4$ (half-rate); and 7) Gaussian channel for comparison.

Interestingly, capacity is rather independent of m for the 3/4- and 1/2-rate STBCs; however, it is generally inferior to the capacity of the full-rate STBCs. Their low dependence is explained with the high diversity already obtained from the three and four transmit antennas. Their low performance comes from the rate loss due to $R < 1$. Furthermore, the Alamouti STBC converges to the Gaussian capacity faster than the one-transmit-antenna case does. It is worth noting that, as long as ergodic Shannon capacity is the system performance measure, distributed communication scenarios under LOS conditions do not yield any significant capacity benefit. However, with unequal link attenuations due to shadowing, the distributed case yields significant benefits, as demonstrated below.

Unequal Channel Gains: Here, the same procedure as for the Rayleigh-fading case is repeated. The MGF $\phi_\lambda(s)$ of the eigenvalue $\lambda = \|\mathbf{h}\|^2$ of the MISO channel with n_{T} transmit antennas can be expressed as

$$\begin{aligned}\phi_\lambda(s) &= \prod_{i=1}^{n_{\mathrm{T}}} \phi_{\lambda_i}(s) \\ &= \frac{1}{\left(1 - s\frac{\alpha_1^2}{m_1}\right)^{m_1}} \cdot \frac{1}{\left(1 - s\frac{\alpha_2^2}{m_2}\right)^{m_2}} \cdots \frac{1}{\left(1 - s\frac{\alpha_{n_{\mathrm{T}}}^2}{m_{n_{\mathrm{T}}}}\right)^{m_{n_{\mathrm{T}}}}}\end{aligned} \tag{37}$$

where m_i is the Nakagami fading parameter of the ith link. Repeating the procedure of the MISO Rayleigh-fading case finally yields, for the capacity

$$C = R\sum_{i=1}^{n_{\mathrm{T}}}\sum_{j=1}^{m_i} K_{i,j} \cdot \frac{1}{\Gamma(j)}\hat{C}_{j-1}\left(\frac{1}{R}\frac{\alpha_i^2}{j n_{\mathrm{T}}}\frac{S}{N}\right) \tag{38}$$

$$= R\sum_{i=1}^{n_{\mathrm{T}}}\sum_{j=1}^{m_i} K_{i,j} \cdot \frac{1}{\Gamma(j)}\hat{C}_{j-1}\left(\frac{\overline{\gamma}_i}{j}\right) \tag{39}$$

where the coefficients $K_{i,j}$ are now found by performing partial fractions on (37).

Fig. 8 depicts the normalized Shannon capacity in natural units per second per Hertz versus the normalized power in the first link α_1^2 over a Nakagami fading channel for the distributed Alamouti scheme: $S/N = 10$ dB and $m = 10$. Again, depicted are the cases where communication happens only over either of the single links, where $\alpha_2^2 = 2 - \alpha_1^2$. Clearly, the region where the distributed Alamouti scheme outperforms the stronger link has reduced to a single point for $\alpha_1^2 = 1$. Furthermore, the capacity of the distributed scenario is up to 15% lower than that of the stronger single-link case. However, the capacity of the distributed scenario is virtually independent of the fading

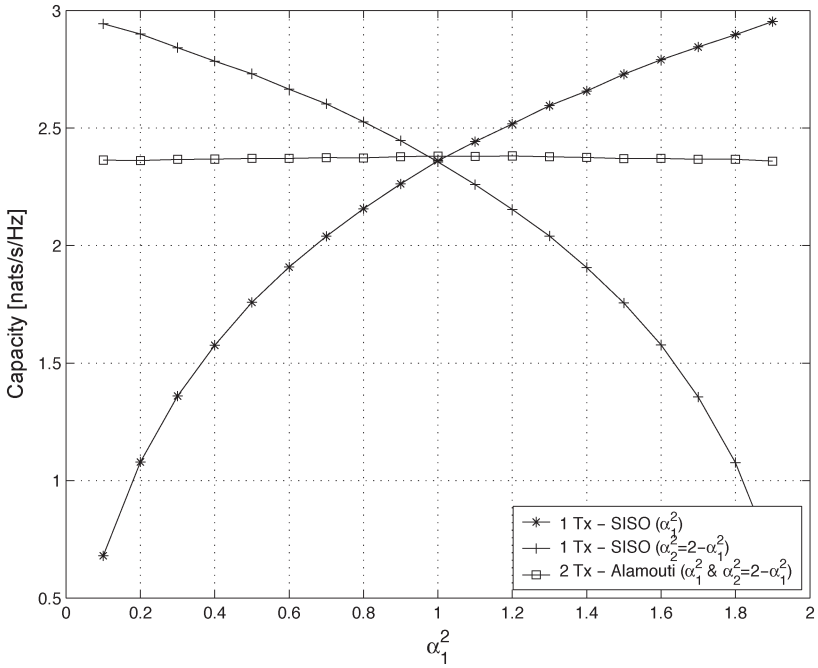

Fig. 8. Normalized Shannon capacity in natural units per second per Hertz versus the normalized power in the first link α_1^2 for the distributed Alamouti scheme over an MISO Nakagami channel. $S/N = 10$ dB and $m = 10$.

coefficients. Therefore, if the sensors are potentially shadowed, then the distributed communication scenario offers significant performance stability.

Generic Channel Gains: The case of generic channel coefficients is similarly obtained as for the Rayleigh channel and is thus omitted here.

IV. Outage Capacity of Orthogonalized Distributed MISO Channels

Given each realization of the MISO channel $\mathbf{h}$ to be memoryless or ergodic, the maximum mutual information is referred to as capacity [39]. To achieve this capacity, codebook entries of infinite length and given capacity-maximizing covariance have to be generated. The capacity of such channels has been dealt with in the previous section. Here, the case of nonergodic channels is analyzed—in particular, the case where the channel realizations are randomly fixed at the beginning of the transmission and kept constant over the infinite transmission duration. The requirement on the infinite length of the codebook entries can be loosened; the performance can then be quantified with the aid of the random coding theory [39]. It can be shown that for increasing code length, the upper capacity bound is reached exponentially. Practically, this implies that the codes deployed by the sensors can be of finite (and comparably short) length without losing too much in performance.

Since the channel realization $\mathbf{h}$ is chosen randomly and kept constant over the codeword transmission, there is a nonzero probability that a given transmission rate R_{C} cannot be supported by the channel [39]. However, the probability that a certain communication rate R_{C} can be supported by a channel $\mathbf{h}$ with average codeword power S can be gauged and is referred to as the outage probability $P_{\mathrm{out}}(R_{\mathrm{C}}, S, \mathbf{h})$. It is therefore the aim to maximize P_{out} for a given channel, average codeword power, and required communication rate. That can be achieved by choosing suitable codewords $\mathbf{x}$ with a given covariance matrix $Q = \mathrm{E}\{\mathbf{x}\mathbf{x}^{\mathbf{H}}\}$, so that $P_{\mathrm{out}}(R_{\mathrm{C}}, S, \mathbf{h})$ equates $\inf\{\text{probability}(\log\det(\mathbf{I} + \mathbf{h}Q\mathbf{h}^{\mathbf{H}}) < R_{\mathrm{C}})\}$ subject to $Q : Q > 0,\ \mathrm{tr}(Q) \leq S$ [39], where $\mathbf{I}$ is the unit matrix. Furthermore, in [39, Ex. 6], it has been shown that if the rank of $\mathbf{h}\mathbf{h}^{\mathbf{H}}$ is 1, then $Q = S$ is optimal. That allows one to derive closed-form expressions for the outage probabilities for various channels by evaluating the channel outage probability induced by the randomness of the instantaneous channel power, here $\mathbf{h}\mathbf{h}^{\mathbf{H}} = \|\mathbf{h}\| = \lambda$, with the appropriate bounds

$$P_{\mathrm{out}}(R_{\mathrm{C}}, S, \mathbf{h}) = \int_0^{\lambda_{R_{\mathrm{C}}}} f_\lambda(\lambda) d\lambda \tag{40}$$

where, with reference to (5), $\lambda_{R_{\mathrm{C}}} = (\mathrm{e}^{R_{\mathrm{C}}/R} - 1)[(1/R)(1/n_{\mathrm{T}})(S/N)]^{-1}$.

A. Orthogonalized MISO Outage Capacity—Rayleigh Fading

Equal Channel Gains: Computing (40) for the Rayleigh fading channel with the pdf given by (16), one obtains

$$P_{\mathrm{out}}(R_{\mathrm{C}}, S, \mathbf{h}) = \frac{1}{\Gamma(n_{\mathrm{T}})}\gamma\left(n_{\mathrm{T}}, \frac{\mathrm{e}^{\frac{R_{\mathrm{C}}}{R}} - 1}{\overline{\gamma}}\right) \tag{41}$$

where $\gamma(a, x) \triangleq \int_0^x \lambda^{a-1}\mathrm{e}^{-\lambda} d\lambda$ is the lower incomplete Gamma function and $\overline{\gamma} = (1/R)(\alpha^2/n_{\mathrm{T}})(S/N)$.

Fig. 9 depicts the rate outage probability in percent versus the rate in natural units per second per Hertz for various STBCs

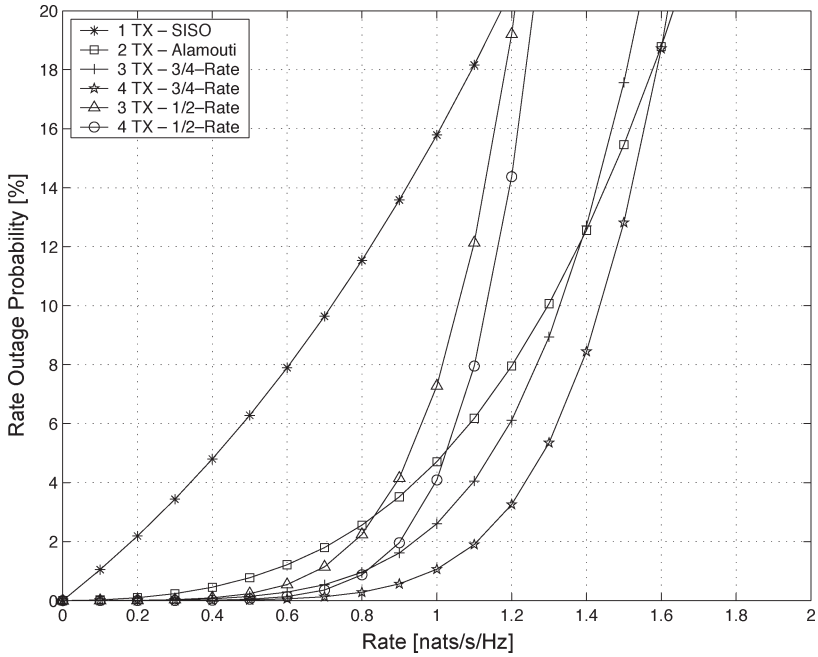

Fig. 9. Outage probability of a given communication rate in percent versus this rate in natural units per second per Hertz for various STBCs over Rayleigh fading channels. $S/N = 10$ dB.

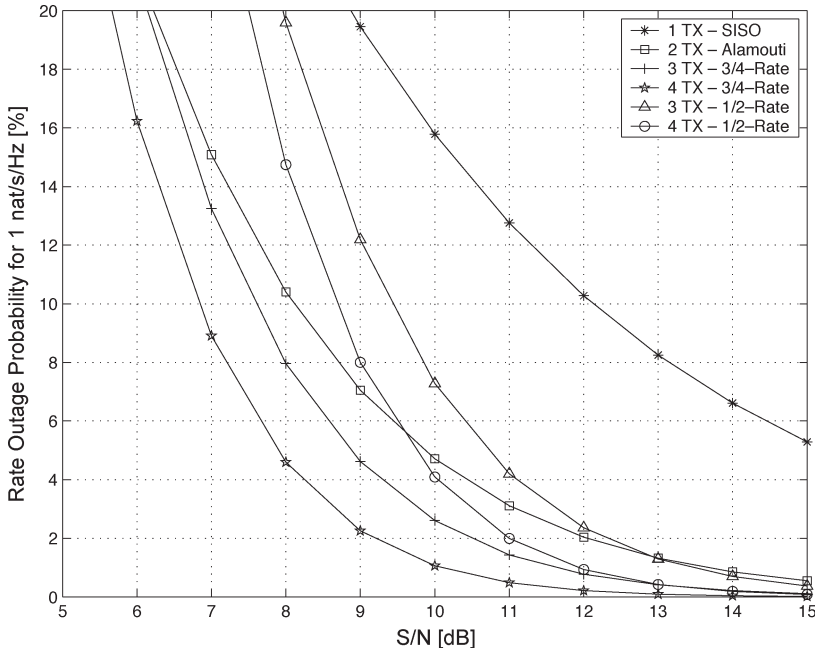

Fig. 10. Outage probability of a given communication rate of 1 nat/s/Hz in percent versus S/N in decibels for various STBC scenarios over Rayleigh fading channels.

over Rayleigh fading channels at $S/N = 10$ dB. Of interest is usually an outage probability of 10%, which means that the channel can support a given rate with a probability of 90%. Clearly, the SISO case performs worst as it supports only 0.7 nats/s/Hz for a 10% outage probability. The half-rate STBCs perform slightly better, achieving gains of approximately 1.05 nats/s/Hz (three transmit) and 1.15 nats/s/Hz (four transmit). Interestingly, the full-rate Alamouti scheme does not yield best performance as for the ergodic channel capacity. It achieves 1.3 nats/s/Hz at 10% outage, whereas the 3/4-rate codes yield approximately 1.35 nats/s/Hz (three antennas) and 1.45 nats/s/Hz (four antennas).

Fig. 10 depicts the rate outage probability in percent versus S/N in decibels for various STBC scenarios over Rayleigh fading channels, which is required to support a fairly low rate of 1 nat/s/Hz. The same observations as above can be made. The gains of the distributed sensor networks over the SISO communication scenario for an outage of 10% are 2.5 dB (1/2 rate, three transmit antennas), 3.3 dB (1/2 rate, four transmit antennas), 4.0 dB (Alamouti, two transmit antennas),

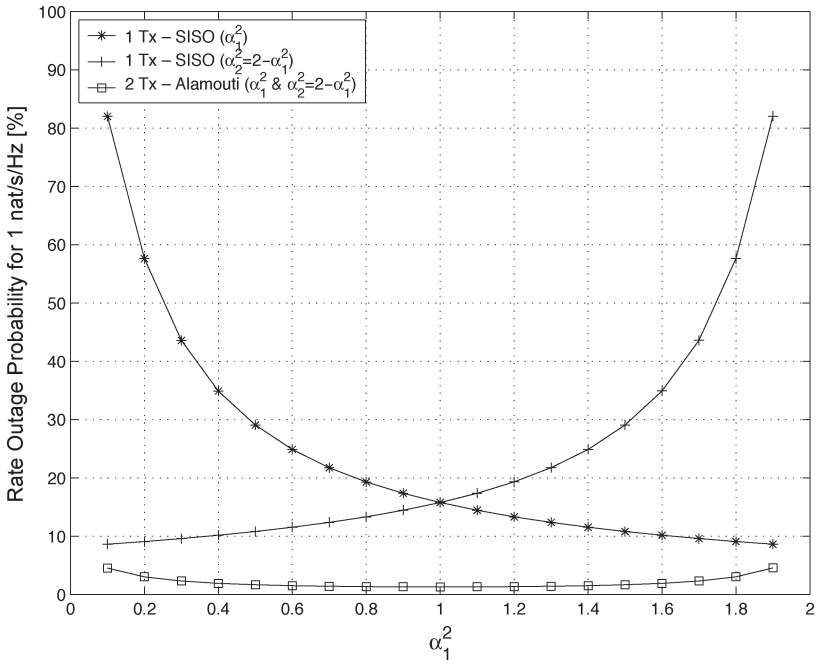

Fig. 11. Outage probability of a given communication rate of 1 nat/s/Hz in percent versus the normalized power in the first link α_1^2 for the distributed Alamouti scheme. $S/N = 10$ dB.

4.5 dB (3/4 rate, three transmit antennas), and 5.3 dB (3/4 rate, four transmit antennas). It is worth noting that the gains decrease for increasing data rates.

A 5.3-dB gain translates to approximately 70% power savings. In contrast to the ergodic channels, it is thus worth deploying distributed sensor networks with more than two distributed transmit antennas per sensor tier for nonergodic channel realizations.

Unequal Channel Gains: Computing (40) for the Rayleigh fading channel with the pdf given by (23), one obtains

$$P_{\text{out}}(R_{\text{C}}, S, \mathbf{h}) = \sum_{i=1}^{n_{\text{T}}} K_i \cdot \left(1 - \text{e}^{-\frac{\text{e}^{\frac{R_{\text{C}}}{R}}-1}{\overline{\gamma_i}}}\right) \qquad (42)$$

where the coefficients K_i are given by (22) and $\overline{\gamma_i} = (1/R)(\alpha_i^2/n_{\text{T}})(S/N)$. The generic case with repeated γ_i is similarly obtained by utilizing the appropriate pdf previously derived.

Fig. 11 depicts the rate outage probability in percent versus the normalized power in the first link α_1^2 for the distributed Alamouti scheme with $S/N = 10$ dB and a desired communication rate of 1 nat/s/Hz. Again, depicted are the cases where communication happens only over either of the single links, where $\alpha_2^2 = 2 - \alpha_1^2$.

Similar to the ergodic case, the outage probability of the distributed scheme is much less dependent on the power of the individual links than the single-link schemes. Furthermore, for the chosen system parameters, the distributed scheme can support a rate of 1 nat/s/Hz with an outage probability of less than 10% for any α_1^2. The single links, however, cannot guarantee this data rate at 10% outage probability for most α_1^2. It can thus be concluded that in the case of independent shadowing between the nodes, a distributed communication scenario will always bring benefits in terms of power savings or rate outage probabilities when compared to a single-link communication scenario.

B. Orthogonalized MISO Outage Capacity—Nakagami Fading

Equal Channel Gains: Computing (40) for the Nakagami m fading channel with the pdf given by (34), one obtains

$$P_{\text{out}}(R_{\text{C}}, S, \mathbf{h}) = \frac{1}{\Gamma(n_{\text{T}}m)}\gamma\left(n_{\text{T}}m, \frac{\text{e}^{\frac{R_{\text{C}}}{R}}-1}{\frac{\overline{\gamma}}{m}}\right) \qquad (43)$$

where $\overline{\gamma} = (1/R)(\alpha^2/n_{\text{T}})(S/N)$. Fig. 12 depicts the rate outage probability in percent versus S/N in decibels for the 3/4-rate STBC scenario with four distributed transmit antennas over Nakagami fading channels, which is required to support a rate of 1 nat/s/Hz. The Nakagami fading factor was chosen to be $m = (1, 2, 4, 6, 8, 10)$. Increasing the m factor from 1 to 10 leads to a power savings of approximately 2.5 dB at an outage probability of 10%. Compared to the ergodic capacity, where capacity saturates very fast for increasing m, this is a notable power gain.

Unequal Channel Gains: Finally, the outage probability over different MISO Nakagami distributions can similarly be calculated as

$$P_{\text{out}}(R_{\text{C}}, S, \mathbf{h}) = \sum_{i=1}^{n_{\text{T}}}\sum_{j=1}^{m_i} K_{i,j} \cdot \frac{1}{\Gamma(j)}\gamma\left(j, \frac{\text{e}^{\frac{R_{\text{C}}}{R}}-1}{\frac{\overline{\gamma}_i}{j}}\right) \qquad (44)$$

where the coefficients $K_{i,j}$ are found by performing partial fractions on (37), and $\overline{\gamma_i} = (1/R)(\alpha_i^2/n_{\text{T}})(S/N)$.

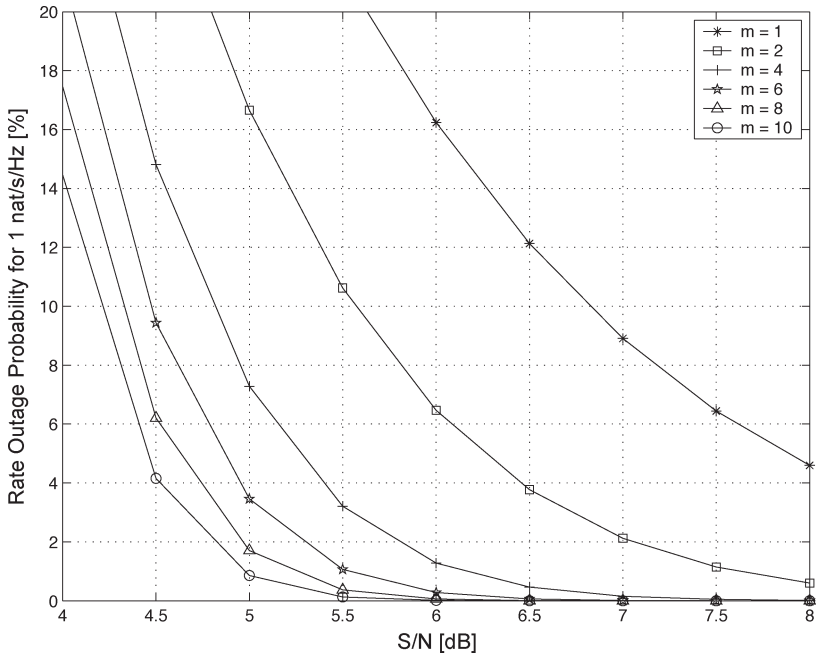

Fig. 12. Outage probability of a given communication rate of 1 nat/s/Hz in percent versus S/N in decibels for the 3/4-rate STBC scenario with four distributed transmit antennas over Nakagami fading channels with $m = (1, 2, 4, 6, 8, 10)$.

V. End-to-End Capacity of Distributed Sensor Networks

A. Theoretical Approach

Fig. 1 depicts the case of a $T + 1$-stage distributed sensor network with T sensor tiers, each acting as a virtual STBC transmit array. The ith sensor tier is assumed to be comprised of d_i sensors, where $i = (1, \ldots, T)$.

The tth stage forms d_{t+1} MISO channels with d_t distributed transmit antennas. The first stage is formed by the s-S, which possesses only one transmit antenna. The $(T + 1)$th stage reaches the t-S and therefore forms only one MISO channel. The capacity of each stage is denoted by $C^{(t)}_{d_t,j}$, where $t = (1, \ldots, T + 1)$ and $j = (1, \ldots, d_t)$. Since the output of an MISO channel is a fractional input to the consecutive MISO channel, the capacity is clearly dominated by the weakest link in the system. Therefore, the end-to-end capacity C is determined by [41]

$$C = \min\left\{C^{(1)}_{1,1}, \ldots, C^{(1)}_{1,d_1}, C^{(2)}_{d_1,1}, \ldots, C^{(2)}_{d_1,d_2}, \ldots, C^{(T+1)}_{d_T,1}\right\}. \tag{45}$$

To maximize end-to-end capacity, weak MISO links should be excluded; however, this has to be traded off against the loss in capacity for the consecutive tier. An analytical optimization approach is very cumbersome but, however, is possible. The interested reader is referred to approaches suggested in [36] and [37], where an optimum power and bandwidth allocation is suggested in dependence of the prevailing channel conditions as well. The suggested approach therein successfully overcomes the problems associated with the logarithmic capacity Lagrangian, solvable only numerically.

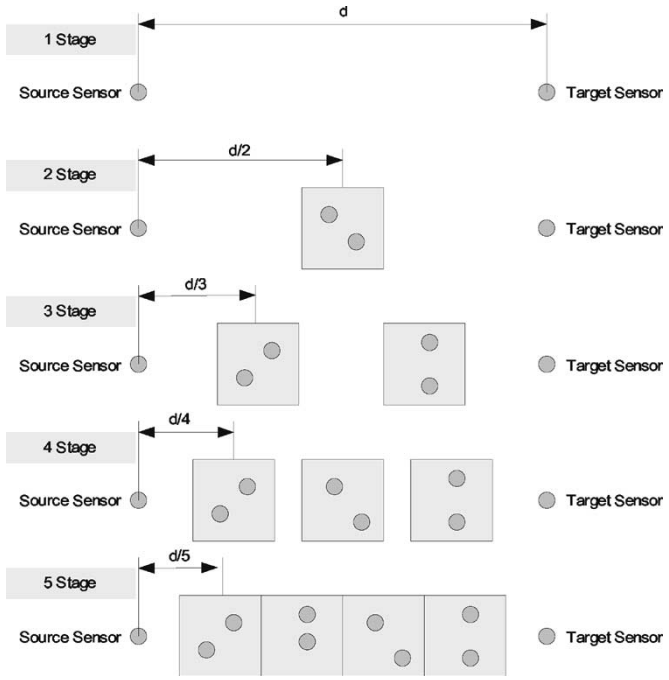

Fig. 13. Multistage distributed sensor network with up to five stages (i.e., four sensor tiers). $d = 100$ m.

B. Simulation Assumptions

A multistage distributed sensor network has been simulated with up to five stages (i.e., four sensor tiers), as depicted in Fig. 13. The distance between the source and target sensors has been kept constant with $d = 100$ m. This scenario could occur, for instance, in an office building where a remote sensor (s-S) reports to a processing central unit (t-S).

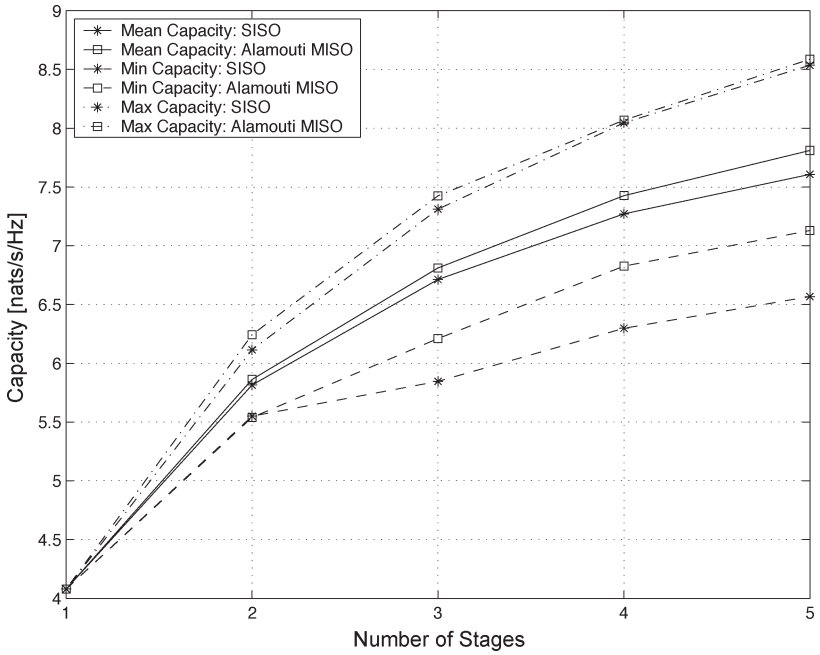

Fig. 14. Normalized minimum, mean, and maximum Shannon capacity in natural units per second per Hertz versus the number of stages utilized. Pathloss index $n = 3$.

The one-stage scenario corresponds to a direct-link communication scenario over 100 m. For the two-stage scenario, the first relaying tier is comprised of various distributed sensors that are randomly located in a squared area of the size $d/5$. Simulated are only full-rate codes; therefore, only one or two distributed sensors are uniformly placed into the shaded area.

The distance between the s-S, the center of the square, and the t-S is $d/2 = 50$ m. For the three-, four-, and five-stage scenarios, the distance between the relaying tiers is chosen to be $d/3 = 33$ m, $d/4 = 25$ m, and $d/5 = 20$ m, respectively. In the five-stage scenario, the sensor distribution areas touch each other; this corresponds to the case when sensors are uniformly distributed along the path between the s-S and t-S.

Furthermore, it is assumed that each sensor transmits an average symbol energy of $E_{\rm s} = 1$ nJ measured at a 1-m distance [42]. The sensor receive noise-power spectral density is assumed to be $N_0 = -140$ dBm/Hz, i.e., a fairly high noise floor due to cheap manufacturing of the sensor nodes. Thus, the resulting $S/N = E_{\rm s}/N_0 = 80$ dB measured at a 1-m distance. Note that an increase in $E_{\rm s}$ or decrease in N_0 only leads to a linear shift of subsequent performance curves.

The pathloss model used is the traditional negative exponential pathloss model where the power loss is inversely proportional to d^n, where d is the distance and n is the pathloss exponent. For the indoor environment, $n \approx (3, \ldots, 6)$, where $n = 3$ and $n = 6$ correspond to lightly and densely cluttered indoor environments, respectively [43].

C. Capacity of Multistage Distributed Sensor Networks

Ergodic Channels Without Shadowing: Figs. 14 and 15 relate to a pathloss coefficient of $n = 3$. Fig. 14 depicts the mean capacity in natural units per second per Hertz versus the number of stages utilized. At each stage, the network performance with and without STBC is compared, where the deployed STBC is the full-rate Alamouti code. Furthermore, the mean, maximum, and minimum capacities have been depicted. Note that there is no fair capacity comparison between the communication scenarios with different stages, as the transmission energy was kept constant per node. If a fair comparison was desired, then the total utilized energy to deliver the information from the s-S to the t-S would have to be equated for all scenarios. Such normalization was not performed here as the primary aim was to compare distributed with traditional sensor networks.

From Fig. 14, it is clear that the capacity of distributed sensor networks is at least as high as for traditional multistage sensor networks. A five-stage distributed sensor network exhibits a 0.25-nats/s/Hz average capacity advantage over the traditional five-stage network. Referring to Fig. 2, this leads to an SNR improvement of approximately 1 dB. As previously stated, the average capacity is a useful performance measure if the communication channels are ergodic.

Since the positions of the sensor nodes are usually fixed, the channels are not ergodic with respect to the location (mean attenuation); however, the channels are still assumed to be ergodic with respect to the fading statistics. Therefore, Fig. 15 depicts the outage probability of the achievable capacity for the chosen uniform sensor distribution.

For the five-stage scenario with uniform sensor distribution at each stage, only 10% of all geometrical sensor distributions cannot support a capacity of 6.7 nats/s/Hz if the traditional SISO scenario is implemented; whereas for the distributed MISO case, all geometrical sensor distributions can support such rate. Only 10% of all five-stage MISO communication scenarios cannot support 7.2 nats/s/Hz. This gives an average capacity advantage of 0.5 nats/s/Hz ($\equiv$ 2 dB) if the respective capacities are to be supported in 90% of all cases.

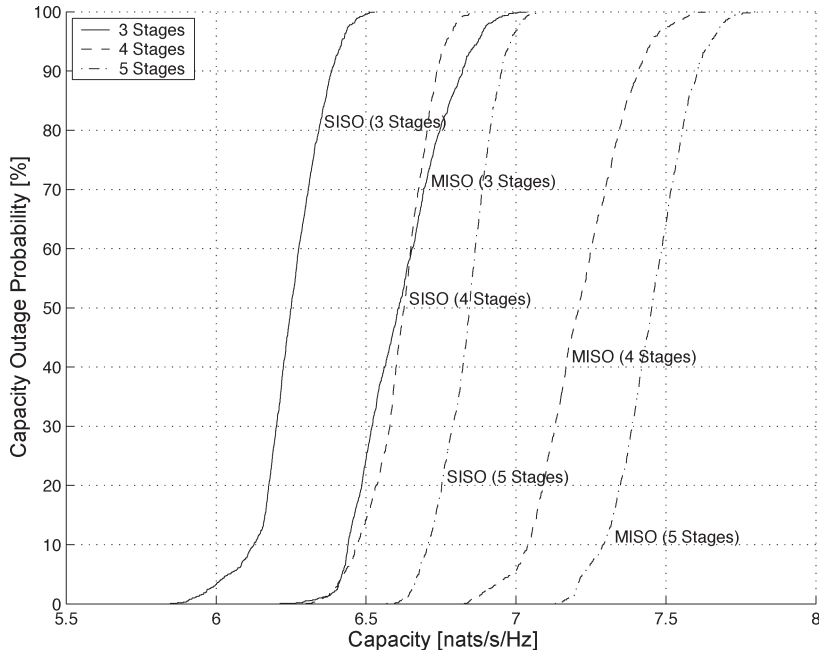

Fig. 15. Outage probability of a given communication rate in percent versus this rate in natural units per second per Hertz for the three-, four-, and five-stage single-antenna and distributed Alamouti sensor-network communication scenarios over Rayleigh fading channels without shadowing. Pathloss index $n = 3$.

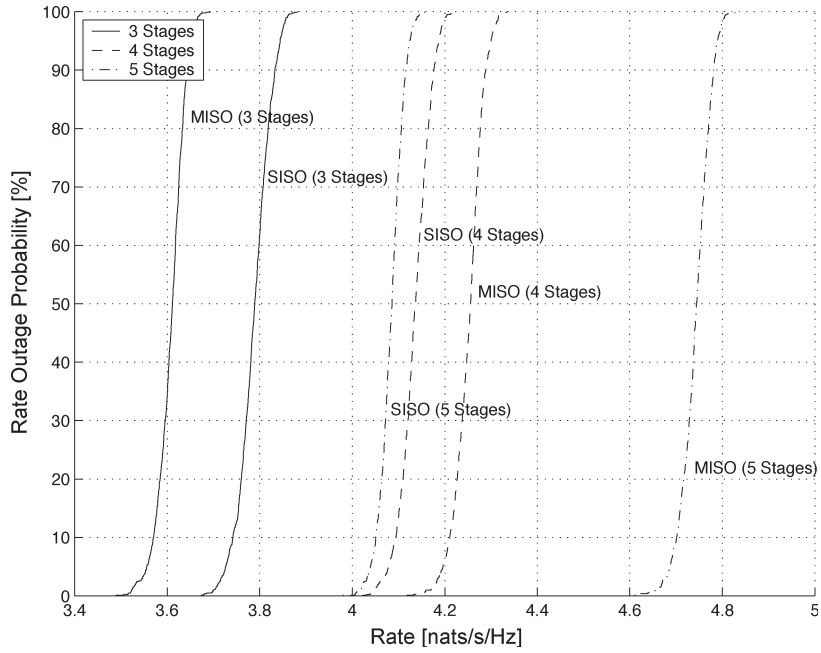

Fig. 16. Outage probability of a given communication rate in percent versus this rate in natural units per second per Hertz for the three-, four-, and five-stage single-antenna and distributed Alamouti sensor-network communication scenarios over Rayleigh fading channels with shadowing. Pathloss index $n = 3$ and shadowing standard deviation $\sigma_{\mathrm{s}} = 0$ dB.

Equivalently, while the distributed communication scenario can support 7.2 nats/s/Hz at 90% of all cases, the traditional sensor network can support such rate only with close to zero probability (i.e., the outage probability is 100%).

The achieved gains of 2 dB translate to transmit power savings of approximately 40%. This clearly corroborates the advantages of distributed communication over traditional SISO communication scenarios.

Nonergodic Channels With Shadowing: The outage probability of the attainable rate is obtained here for the case when each link is effected by independent shadowing. For the Monte Carlo simulations, only a small shadowing standard deviation of 0 dB was assumed.

Fig. 16 depicts the outage probability of the attainable rates versus the rate in natural units per second per Hertz for the three-, four-, and five-stage communication scenarios.

Interestingly, for the chosen sensor distribution, the three-stage distributed communication scenario does not yield any capacity benefits over the SISO case. Furthermore, the four-stage distributed case yields only small gains. Finally, when the sensors are densely and uniformly distributed between the s-S and t-S, only then can drastic gains be observed. The latter case corresponds to anticipated high-density sensor-network layouts.

The five-stage distributed sensor network yields a gain of 0.65 nats/s/Hz for an outage probability of 10%. This mounts to power savings of approximately 3 dB, or 50%.

VI. Conclusion

This paper derived closed-form expressions for the Shannon capacity for sensor networks over distributed ergodic flat-fading Rayleigh and Nakagami channels. Also derived were the respective outage probabilities in the case of nonergodic channel realizations.

STBCs allow a simple implementation and are thus suitable for power-limited sensor nodes. They are known to orthogonalize the multiple-input multiple-output (MIMO) channel, which allows an analytical treatment of various capacity and performance problems. Because each sensor node is assumed to possess only one antenna element, a distributed network can only realize MISO channels. However, the exposed analysis herein is easily extended to the generic MIMO case.

The capacity derivations are based on a closed-form expression of the capacity integral, which was introduced and solved in [37]. It has been utilized to find closed-form expressions for the Shannon capacity over ergodic MISO identically distributed flat-fading Rayleigh and Nakagami channels. In the case that each of the wireless links may have a different attenuation or Nakagami m factor, closed-form capacity expressions are derived by performing partial fractions on the respective MGFs, after which the derivation of the capacity is straightforward. Similarly, the outage probabilities of supportable rates were derived for various configurations.

It has been shown that in the case of ergodic channels, optimum performance is achieved if a distributed Alamouti scheme is deployed. In the case of nonergodic channels, the outage probability for a desired communication rate is minimized if sporadic 3/4-rate STBCs are utilized with four transmit antennas. Gains of up to 5 dB could be observed in the case of a distributed sensor deployment, compared to a traditional single-link communication scenario. This clearly demonstrates the benefit of a distributed communication scenario.

Furthermore, Monte Carlo simulations have been performed to evaluate the average capacity and the associated outage probability for the Alamouti scheme. Again, it could be shown that a distributed deployment generally yields significant performance gains.

Note that sensors cannot operate at Shannon limit due to their limitations on complexity. However, the derived capacity and outage bounds give an indication on the performance of the systems introduced.

Appendix

Following the approach exposed in [44, Ch. 12], it is proven here that

$$K_{i,j} = \frac{1}{(\nu_i - j)!\,(-\alpha_i^2)^{\nu_i - j}} \cdot \frac{\partial^{\nu_i - j}}{\partial s^{\nu_i - j}} \left[\prod_{i'=1, i' \neq i}^{g} \frac{1}{(1 - s\alpha_{i'}^2)^{\nu_{i'}}} \right]_{\frac{s=1}{\alpha_i^2}} \tag{46}$$

if the partial fractions are applied to (25), which, expanded into its partial fractions, can be expressed as

$$\phi_\lambda(s) = \left[\frac{K_{1,1}}{(1 - \alpha_1^2 s)^1} + \cdots + \frac{K_{1,\nu_1}}{(1 - \alpha_1^2 s)^{\nu_1}} \right] + \cdots + \left[\cdots + \frac{K_{g,\nu_g}}{(1 - \alpha_g^2 s)^{\nu_g}} \right]. \tag{47}$$

To obtain coefficient K_{i,ν_i}, (47) is multiplied with $(1 - \alpha_i^2 s)^{\nu_i}$, after which s is set to $s = 1/\alpha_i^2$ to arrive at $K_{i,\nu_i} = \prod_{i'=1, i' \neq i}^{g} (1 - \alpha_{i'}^2/\alpha_i^2)^{-\nu_{i'}}$. Furthermore, to obtain coefficient $K_{i,\nu_i - 1}$, (47) is multiplied with $(1 - \alpha_i^2 s)^{\nu_i}$, differentiated with respect to s, after which s is set to $s = 1/\alpha_i^2$ to arrive at

$$K_{i,\nu_i - 1} = \frac{1}{(-\alpha_i^2)} \frac{\partial}{\partial s} \left[\prod_{i'=1, i' \neq i}^{g} \frac{1}{(1 - s\alpha_{i'}^2)^{\nu_{i'}}} \right]_{\frac{s=1}{\alpha_i^2}}. \tag{48}$$

Hence, coefficient $K_{i,1}$ is obtained by multiplying (47) with $(1 - \alpha_i^2 s)^{\nu_i}$, differentiated $(\nu_i - 1)$ times with respect to s, after which s is set to $s = 1/\alpha_i^2$ to arrive at

$$K_{i,1} = \frac{1}{(\nu_i - 1)!\,(-\alpha_i^2)^{\nu_i - 1}} \cdot \frac{\partial^{\nu_i - 1}}{\partial s^{\nu_i - 1}} \left[\prod_{i'=1, i' \neq i}^{g} \frac{1}{(1 - s\alpha_{i'}^2)^{\nu_{i'}}} \right]_{\frac{s=1}{\alpha_i^2}} \tag{49}$$

which concludes the proof.

Note that the $(\nu_i - j)$th derivative of $\prod_{i'=1, i' \neq i}^{g} (1 - s\alpha_{i'}^2)^{-\nu_{i'}}$ in (46) is easily derived in closed form. To enhance readability, the following symbolic notation is introduced:

$$[\Pi] \triangleq \prod_{i'=1, i' \neq i}^{g} \frac{1}{(1 - s\alpha_{i'}^2)^{\nu_{i'}}} \tag{50}$$

$$[\Sigma] \triangleq \sum_{i'=1, i' \neq i}^{g} \frac{\nu_{i'} \alpha_{i'}^2}{1 - s\alpha_{i'}^2} \tag{51}$$

$$[\Sigma^n] \triangleq \sum_{i'=1, i' \neq i}^{g} \frac{\nu_{i'} \left(\alpha_{i'}^2\right)^n}{(1 - s\alpha_{i'}^2)^n} \tag{52}$$

$$\partial^n [\cdot] \triangleq \frac{\partial^n}{\partial s^n} [\cdot]. \tag{53}$$

With the introduced notation, the following holds:

$$\partial[\Sigma^n] = n[\Sigma^{n+1}] \tag{54}$$

$$\partial[\Sigma]^m = m[\Sigma]^{m-1}[\Sigma^2] \tag{55}$$

and generally

$$\partial[\Xi][\Psi] = \partial[\Xi] \cdot [\Psi] + [\Xi] \cdot \partial[\Psi]. \tag{56}$$

This finally allows one to rewrite the first order and, inductively, any higher order derivative as

$$\partial[\Pi] = [\Pi][\Sigma] \tag{57}$$

$$\begin{aligned}\partial^2[\Pi] &= \partial[\Pi][\Sigma] \\ &= \partial[\Pi] \cdot [\Sigma] + [\Pi] \cdot \partial[\Sigma] \\ &= [\Pi]\left([\Sigma]^2 + [\Sigma^2]\right)\end{aligned} \tag{58}$$

$$\begin{aligned}\partial^3[\Pi] &= \partial\left[[\Pi]\left([\Sigma]^2 + [\Sigma^2]\right)\right] \\ &= \partial[\Pi] \cdot \left([\Sigma]^2 + [\Sigma^2]\right) + [\Pi] \cdot \partial\left([\Sigma]^2 + [\Sigma^2]\right) \\ &= [\Pi]\left([\Sigma]^3 + 3[\Sigma][\Sigma^2] + 2[\Sigma^3]\right)\end{aligned} \tag{59}$$

$$\begin{aligned}\partial^4[\Pi] = [\Pi]&([\Sigma][\Sigma]^3 + 6[\Sigma]^2[\Sigma^2] \\ &+ 8[\Sigma][\Sigma^3] + 3[\Sigma^2]^2 + 6[\Sigma^4])\end{aligned} \tag{60}$$

etc.

ACKNOWLEDGMENT

The authors would like to express their gratitude to the anonymous reviewers for their many valuable comments and suggestions.

REFERENCES

[1] I. F. Akyildiz, W. Su, Y. Sankarasubramaniam, and E. Cayirci, "A survey on sensor networks," *IEEE Commun. Mag.*, vol. 40, no. 8, pp. 102–114, Aug. 2002.

[2] R. C. Shah and J. Rabaey, "Energy aware routing for low energy ad hoc sensor networks," in *Proc. IEEE Wireless Communications and Networking Conf. (WCNC)*, Orlando, FL, Mar. 17–21, 2002, pp. 350–355.

[3] K. Sohrabi, J. Gao, V. Ailawadhi, and G. Pottie, "Protocols for self-organization of a wireless sensor network," *IEEE Pers. Commun.*, vol. 7, no. 5, pp. 16–27, Oct. 2000.

[4] *Wireless Integrated Network Sensors*, Los Angeles, CA: Univ. California. [Online]. Available: http://www.janet.ucla.edu/WINS

[5] J. M. Kahn, R. H. Katz, and K. S. J. Pister, "Next century challenges: Mobile networking for smart dust," in *Proc. Mobile Computing and Networking (MobiCom)*, Seattle, WA, 1999, pp. 483–492.

[6] V. Raghunathan, C. Schurgers, S. Park, and M. B. Srivastava, "Energy aware wireless microsensor networks," *IEEE Trans. Signal Process.*, vol. 19, no. 2, pp. 40–50, Mar. 2002.

[7] E. Shih *et al.*, "Physical layer driven algorithm and protocol design for energy-efficient wireless sensor networks," in *Proc. ACM Mobile Computing and Networking (MobiCom)*, Rome, Italy, Jul. 2001, pp. 272–286.

[8] G. J. Pottie and W. J. Kaiser, "Wireless integrated network sensors," *Commun. ACM*, vol. 43, no. 5, pp. 51–58, May 2000.

[9] M. Ahmed, Y.-S. Tu, and G. Pottie, "Cooperative detection and communication in wireless sensor networks," in *Proc. 38th Allerton Conf. Communication, Control, and Computing*, Urbana, IL, Oct. 4–6, 2000, pp. 755–764.

[10] A. Woo and D. E. Culler, "A transmission control scheme for media access in sensor networks," in *Proc. ACM Mobile Computing and Networking (MobiCom)*. Rome, Italy, Jul. 2001, pp. 221–235.

[11] A. Salhieh and L. Schwiebert, "Power aware metrics for wireless sensor networks," in *Proc. IASTED Conf. Parallel and Distributed Computing and Systems (PDCS) Symp.*, Cambridge, MA, Nov. 2002, pp. 326–331.

[12] A. Sinha and A. Chandrakasan, "Dynamic power management in wireless sensor networks," *IEEE Des. Test Comput.*, vol. 18, no. 2, pp. 62–75, Mar./Apr. 2001.

[13] J. N. Laneman, G. W. Wornell, and D. N. C. Tse, "An efficient protocol for realizing cooperative diversity in wireless networks," in *Proc. IEEE Int. Symp. Information Theory (ISIT)*, Washington, DC, Jun. 2001, p. 294.

[14] P. Gupta and P. R. Kumar, "Towards an information theory of large networks: An achievable rate region," in *Proc. IEEE Int. Symp. Information Theory (ISIT)*. Washington, DC, Jun. 2001, p. 150.

[15] A. Reznik, S. Kulkarni, and S. Verdu, "Capacity and optimal resource allocation in the degraded Gaussian relay channel with multiple relays," in *Proc. Allerton Conf. Communications, Control, and Computing*, Monticello, IL, Oct. 2002. CD-ROM.

[16] A. Sendonaris, E. Erkip, and B. Aazhang, "User cooperation diversity—Part I: System description," *IEEE Trans. Commun.*, vol. 51, no. 11, pp. 1927–1938, Nov. 2003.

[17] ——, "User cooperation diversity—Part II: Implementation aspects and performance analysis," *IEEE Trans. Commun.*, vol. 51, no. 11, pp. 1939–1948, Nov. 2003.

[18] J. N. Laneman, D. N. C. Tse, and G. W. Wornell, "Cooperative diversity in wireless networks: Efficient protocols and outage behavior," *IEEE Trans. Inf. Theory*, vol. 50, no. 12, pp. 3062–3080, Dec. 2004.

[19] J. N. Laneman and G. W. Wornell, "Distributed space–time coded protocols for exploiting cooperative diversity in wireless networks," *IEEE Trans. Inf. Theory*, vol. 49, no. 10, pp. 2415–2525, Oct. 2003.

[20] Y. Tang and M. C. Valenti, "Coded transmit macrodiversity: Block space–time codes over distributed antennas," in *Proc. IEEE Vehicular Technology Conf. (VTC)*, Rhodes, Greece, May 2001, pp. 1435–1438.

[21] T. E. Hunter and A. Nosratinia, "Cooperation diversity through coding," in *Proc. IEEE Int. Symp. Information Theory (ISIT)*, Lausanne, Switzerland, Jul. 2002, p. 220.

[22] A. Stefanov and E. Erkip, "On the performance analysis of cooperative space–time coded systems," in *Proc. IEEE Wireless Communications and Networking Conf. (WCNC)*, New Orleans, LA, Mar. 2003, vol. 2, pp. 729–734.

[23] P. A. Anghel, G. Leus, and M. Kavehl, "Multi-user space–time coding in cooperative networks," in *Proc. IEEE Int. Conf. Acoustics, Speech, and Signal Processing (ICASSP)*, Hong Kong, Apr. 2003, vol. 4, pp. 73–76.

[24] Y. Hua, Y. Mei, and Y. Chang, "Wireless antennas—Making wireless communications perform like wireline communications," in *Proc. IEEE Topical Conf. Wireless Communication Technology*, Honolulu, HI, Oct. 15–17, 2003, pp. 1–27.

[25] A. Stefanov and E. Erkip, "Cooperative coding for wireless networks," in *Proc. 4th IEEE Conf. Mobile and Wireless Communication Networks*, Stockholm, Sweden, Sep. 2002, pp. 273–277.

[26] S. M. Alamouti, "A simple transmit diversity technique for wireless communications," *IEEE J. Sel. Areas Commun.*, vol. 16, no. 8, pp. 1451–1458, Oct. 1998.

[27] V. Tarokh, H. Jafarkhani, and A. Calderbank, "Space–time block codes from orthogonal design," *IEEE Trans. Inf. Theory*, vol. 45, no. 5, pp. 1456–1466, Jul. 1999.

[28] V. Tarokh, H. Jafarkhani, and A. R. Calderbank, "Space–time block coding for wireless communications: Performance results," *IEEE J. Sel. Areas Commun.*, vol. 17, no. 3, pp. 451–460, Mar. 1999.

[29] V. Tarokh, N. Seshadri, and A. Calderbank, "Space time codes for high data rate wireless communication: Performance criterion and code construction," *IEEE Trans. Inf. Theory*, vol. 44, no. 2, pp. 744–765, Mar. 1998.

[30] G. J. Foschini, "Layered space–time architecture for wireless communication in a fading environment when using multi-element antennas," *Bell Labs Tech. J.*, vol. 1, no. 2, pp. 41–59, Autumn 1996.

[31] H. Shin and J. H. Lee, "Exact symbol error probability of orthogonal space–time block codes," in *Proc. IEEE Global Telecommunications (GLOBECOM)*, Taipei, Taiwan, Nov. 17–21, 2002, pp. 1547–1552.

[32] R. U. Nabar, H. Bölcskei, and A. J. Paulraj, "Diversity and outage performance in space–time block coded Ricean MIMO channels," *IEEE Trans. Wireless Commun.*, vol. 4, no. 5, pp. 2519–2532, Sep. 2005.

[33] E. G. Larsson and P. Stoica, *Space–Time Block Coding for Wireless Communications*. Cambridge, U.K.: Cambridge Univ. Press, 2003.

[34] M. Dohler, F. Said, A. Ghorashi, and H. Aghvami, *Improvements in or Relating to Electronic Data Communication Systems*. Publication No. WO 03/003672, priority date 28 June 2001.

[35] M. Dohler, A. Gkelias, and H. Aghvami, "2-hop distributed MIMO communication system," *Electron. Lett.*, vol. 39, no. 18, pp. 1350–1351, Sep. 2003.
[36] ——, "A resource allocation strategy for distributed MIMO multi-hop communication systems," *IEEE Commun. Lett.*, vol. 8, no. 2, pp. 99–101, Feb. 2004.
[37] M. Dohler, "Virtual antenna arrays," Ph.D. dissertation, Centre for Telecommunications Research, Univ. London, London, U.K., 2003.
[38] J. Proakis, *Digital Communications*, 4th ed. New York: McGraw-Hill, 2000.
[39] E. Telatar, "Capacity of multi-antenna Gaussian channels," *Eur. Trans. Telecommun.*, vol. 10, no. 6, pp. 585–595, Nov./Dec. 1999.
[40] M. K. Simon and M.-S. Alouini, *Digital Communication Over Fading Channels*. New York: Wiley, 2000.
[41] T. Cover and J. A. Thomas, *Elements of Information Theory*. New York: Wiley, 1991.
[42] T. Basten, L. Benini, A. Chandrakasan, M. Lindwer, J. Liu, R. Min, and F. Zhao, "Scaling into ambient intelligence," in *Proc. Design, Automation, and Test Europe*, Munich, Germany, Mar. 2003, pp. 76–81.
[43] R. Vaughan and J. B. Andersen, *Channels, Propagation and Antennas for Mobile Communications, Electromagnetic Wave Series*. London, U.K.: IEE, 2003.
[44] J. W. Nilsson and S. A. Ridel, *Electric Circuits*, 6th ed. Upper Saddle River, NJ: Prentice-Hall, 2000.

Mischa Dohler (S'99–M'04) received the M.Sc. degree in telecommunications from King's College London, London, U.K., in 1999, the Diploma degree in electrical engineering from Dresden University of Technology, Dresden, Germany, in 2000, and the Ph.D. degree from King's College London in 2003.

He was a lecturer at the Centre for Telecommunications Research, King's College London, until June 2005. He is now in the R&D department of France Telecom, Paris, France, working on embedded and future communication systems. Prior to Telecommunications, he studied physics in Moscow, Russia. He has won various competitions in mathematics and physics and participated in the Third round of the International Physics Olympics for Germany.

Dr. Dohler has been the Student Representative of the IEEE UKRI Section, a member of the Student Activity Committee of IEEE Region 8, and the London Technology Network Business Fellow for King's College London. He has published over 50 technical journal and conference papers, holds several patents, co-edited and contributed to several books, and has given numerous international short-courses. He has been TPC member and co-chair of various conferences and is member of the editorial board of the *EURASIP Journal*.

Athanasios Gkelias (S'02) received the degree from the Department of Electrical and Computer Engineering, Aristotle University of Thessaloniki, Greece (AUTH), in 2000. In 2001, he received the M.Sc. degree in telecommunications from King's College, University of London, London, U.K. He is currently working toward the Ph.D. degree at the Centre for Telecommunication Research, King's College London.

His research interest lies in the area of *ad hoc* and sensor networks, particularly in the performance analysis and design of medium access control (MAC) protocols.

A. Hamid Aghvami (M'87–SM'91–F'04) joined the academic staff at King's College, London, in 1984. In 1989, he was promoted to Reader and to Professor in Telecommunications Engineering in 1992. He was Visiting Professor at NTT Radio Communication Systems Laboratories in 1990 and Senior Research Fellow at BT Laboratories in 1998–1999. He is currently the Director of the Centre for Telecommunications Research at King's College, London, U.K. He carries out consulting work on Digital Radio Communications Systems for both British and International companies. He has published over 300 technical papers and given invited talks all over the world on various aspects of Personal and Mobile Radio Communications, as well as giving courses on the subject worldwide. He is currently an Executive Advisor to Wireless Facilities Inc., and Managing Director of Wireless Multimedia Communications, Ltd. (his own consultancy company). He leads an active research team working on numerous mobile and personal communications projects for third- and fourth-generation systems, and these projects are supported both by the government and industry.

Prof. Aghvami is a distinguished lecturer and a member of the Board of Governors of the IEEE Communications Society. He has been member, Chairman, and Vice-Chairman of the Technical Program and Organizing Committees of a large number of international conferences. He is also a founder of the International Conference on Personal Indoor and Mobile Radio Communications (PIMRC). He is a Fellow of the Royal Academy of Engineering and IEE.